

An electrochemical sensor based on MnO₂ nanostructures modified reduced graphene oxide (rGO) for detection of dopamine

Meng Lu^{1,2,3}, Wenzhao Luo⁴, Yuhui Zhou⁵, Mishan Wu^{1,2,*}

¹ Hebei Key Laboratory of Chinese Medicine Research on Cardio-Cerebrovascular Disease, Shijiazhuang, 050091, China

² Department of Formulaology, Basic Medicine College, Hebei University of Chinese Medicine, Shijiazhuang, 050200, China

³ Academy of Traditional Chinese Medicine, Henan University of Chinese Medicine, Zhengzhou 450046, China

⁴ Department of Liver, Spleen and Stomach Diseases, Henan Province Hospital of Traditional Chinese Medicine, Zhengzhou, 450002, China

⁵ Digestive System Department, Tangshan Hospital of Traditional Chinese Medicine, Tangshan, 063000, China

*E-mail: mishan_wu@yeah.net

Received: 29 May 2021/ Accepted: 19 July 2021 / Published: 10 September 2021

This study was performed to fabricate the electrochemical dopamine sensor based on MnO₂ nanostructures modified reduced graphene oxide (MnO₂/rGO) electrode in the pharmaceutical sample. The GO nanosheets were synthesized using modified Hummers technique for modification of the glassy carbon electrode (GCE), and then reduced using the electrochemical technique. MnO₂ nanostructures were electrochemically deposited on rGO/GCE. The structural characterization using SEM and XRD showed the vertical growth of tetragonal crystalline of α -MnO₂ nanoplates on crumpled rGO nanosheets. The electrochemical studies using CV, and DPV indicated to higher electroactive surface area of MnO₂/rGO/GCE and its higher sensitivity to the determination of dopamine than that on GCE, rGO/GCE and MnO₂/GCE because of the synergetic effect of rGO nanosheets and high porous and sharp tips of MnO₂ nanoplates. The amperometric studies showed that the sensitivity, detection limit and linear range of MnO₂/rGO/GCE were obtained at 0.28808 μ A/ μ M, 0.002 μ M and 0 to 1100 μ M, respectively. The interference effect on the determination of dopamine showed the great selectivity of MnO₂/rGO/GCE using the amperometry technique at 0.11V. The practical feasibility of MnO₂/rGO/GCE as a dopamine sensor was evaluated in dopamine hydrochloride injection as a pharmaceutical product and results showed the good agreements between the electrochemical analysis and clinical laboratory data. Finally, the acceptable values of recovery (> 98.2%) and relative standard derivation (<3.91%) of the analytical analysis showed that the proposed dopamine sensor can be used as a precise and reliable sensor in complicated pharmaceutical samples.

Keywords: Dopamine; Electrochemical Sensor; MnO₂ nanoplates; Reduced Graphene oxide; Amperometry

1. INTRODUCTION

Alzheimer's disease is an irreversible and progressive neurologic disorder that leads to the death of brain cells and shrinkage of different areas of the brain. As consequence, it causes dementia, memory loss and cognitive decline [1, 2]. In Alzheimer's disease, dementia symptoms are usually appeared slowly and progressively worsen over time [3]. In its early stages, memory problems are typically one of the first signs of Alzheimer's disease [4, 5]. In late-stage Alzheimer's, decline in thinking, behavioral and social skills that affect a person's ability to function independently and individuals lose the ability to carry on a conversation and respond to their environment [6, 7]. This disease is the sixth-leading cause of death in the United States and the fifth-leading cause of death among that age 65 and older [8, 9].

There's no cure for Alzheimer's, but one treatment may potentially delay decline from the disease, and there are drug and non-drug options that may help treat. Medications called cholinesterase inhibitors are prescribed for mild to moderate Alzheimer's disease [10, 11]. These drugs may help reduce some symptoms and help control some behavioral symptoms. Recent studies showed low dopamine levels may mean an increased risk of Alzheimer's disease. The drug which acts on dopamine transmission in the brain improves frontal cognitive function in patients with mild-to-moderate Alzheimer's disease [12, 13].

Dopamine (4-(2-aminoethyl)benzene-1,2-diol) as an organic chemical catecholamine and phenethylamine families is a neurotransmitter that plays several important roles in the brain and body [14]. Dopamine constitutes about 80% of the catecholamine content in the brain. Researchers have found that loss of dopamine may be part of the reason why people with Alzheimer's disease have less effective memories [15]. Highly sensitive MRI scans showed a potential link between dopamine and a part of the brain that may impact the future of Alzheimer's diagnosis. The dopamine found in the ventral tegmental area (VTA) is a chemical that plays a role in reward-motivated behavior, and helps to control movement and form new memories. De Marco and Venneri [16] studied VTA and how it's linked to the hippocampus which is a key part of the brain that helps create memories. Their results showed that there was a link between the size and functionality of the dopamine-rich VTA, the size of the hippocampus, and the ability to learn new information. The smaller size of the VTA meant a smaller amount of dopamine going to the hippocampus which resulted in decreased memory performance [17].

Accordingly, determination of dopamine levels in blood, urine and medicinal drugs is important, and many researchers have been conducted on synthesis, identify and determination of dopamine levels in biological media and pharmaceutical samples using fluorimetry, fluorescence spectroscopy, mass spectrometry, flame emission spectrophotometry, chemiluminometry, atomic absorption, high-pressure liquid chromatography, spectrofluorimetry and electrochemistry techniques [18-21]. Fabrication of high reproducible and selective sensors is necessary due to low level of dopamine in biological samples and the presence of different substances [22, 23]. Many detecting techniques of dopamine lack the stability of selectivity. Therefore, this study was performed to

fabrication the selective and low detection limit electrochemical dopamine sensor based on MnO₂ nanostructures modified reduced graphene oxide electrode in the pharmaceutical sample.

2. EXPERIMENTAL

2.1 Synthesis of nanostructured modified electrodes

Prior to the experiments, the GCE (3 mm, Tianjin Aida Hengsheng Technology Development Co., Ltd., China) was successively polished on micro cloth pads using 0.30 μ m and 0.05 μ m alumina powder and washed carefully with ethanol and distilled water, respectively. Subsequently, it was immersed in a mixture of 1M H₂SO₄ (98%, Huaqiang Chemical Group Stock Co., Ltd., China) and H₂O₂ (30%, Merck, Germany) in a volume ratio of 1:3 for 10 minutes, and rinsed with distilled water, and dried in air.

GO was synthesized using modified Hummers method [24, 25]. 10g of graphite powder (99%, Topfly Material Co., Ltd., China) was incorporated into the of 250 mL sulfuric acid (99%, Merck, Germany) in ice bath for 30 minutes, followed by the addition of 30g KMnO₄ (\geq 99.0%, Merck, Germany) and 300 mL distilled water under magnetic-stirring for 100 minutes at 33°C. The resulted product was set for 4 days. Next, 400mL distilled water and 25mL H₂O₂ were ultrasonically added to the suspension. After 60 minutes of ultrasonication treatment, the obtained mixture was filtered and ultrasonically washed using 1M HCl (37%, Sigma-Aldrich) solution and distilled water, respectively. After then, the obtained suspension was centrifuged at 1000rpm for 20 minutes and dried in an oven for 24 hours at 75°C.

For the preparation of rGO/GCE, 20 mg of the obtained GO was ultrasonically exfoliated in 20 mL distilled water for 60 minutes. The main oxygen-containing functional groups are distributed on GO nanosheets [26]. 10 μ L of GO the suspension was dropped onto the GCE surface and dried at room temperature for 2 hours. The electrochemical reduction of the GO nanosheet on GCE was carried out in a potentiostat using an electrochemical cell with a standard three-electrodes cell which contained the prepared sample, Ag/AgCl(3MKCl) and Pt plate as working, reference and auxiliary electrodes, respectively [27]. The GO/GCE was cycled thrice between a potential ranges from -0.85 V to 0.75 V at scan rate of 20 mV/s in 0.1 phosphate buffer solution (PBS) pH 3.0.

The rGO/GCE and GCE surfaces were modified with MnO₂ nanostructures through the electrodeposition process [28]. Electrodeposition was conducted on Autolab with potentiostat under the potential of -0.1 to 0.6 V at a scan rate of 15mV/s for 12 minutes at room temperature. The electrodeposition electrolyte was prepared from a mixture of 0.5 M KMnO₄ and 2 mM NaNO₂ (\geq 97.0%, Merck, Germany) aquatic solutions in equal volume ratio and the pH were adjusted to 2 using concentrated HCl.

2.2 Structural and electrochemical analyses methods

CV, DPV and amperometry experiments were carried out using the Autolab with potentiostat in 0.1 M PBS pH 7 which prepared from a mixture of 0.1M Na₂HPO₄ (\geq 99.0%, Merck, Germany) and 0.1M NaH₂PO₄ (99%, Merck, Germany) in equal ratio. In order to prepare the real sample,

dopamine hydrochloride injection (40mg/mL) was used as a pharmaceutical real sample. Dopamine hydrochloride injection was provided from the local pharmacy and added to 0.1 M PBS in an equal volume ratio. The sample was kept in a refrigerator at 5°C for electrochemical studies.

Structural characterization of prepared nanomaterial was performed using scanning electron microscopy (SEM, SUPR40, Carl Zeiss AG, Oberkochen, Germany) and X-ray diffraction (XRD; D5005, Siemens AG, Munich, Germany) with 1.5404 Å (Cu K α).

3. RESULTS AND DISCUSSION

3.1 Structural and morphological studies

Figure 1 presents the SEM image of the electrodeposited MnO₂ NRs on smooth surface of GCE. As observed from Figure 1a, the tetragonal nanorods with average lengths of 700nm and average diameter of 50nm were deposited on electrode surface. Notwithstanding the initial nucleation of nanorods is in uniform distribution, agglomeration can be observed in some cases which may be related to the growth of the nanorods upon one another at repeated cycles during electrodeposition process [29]. Figure 1b shows the surface of rGO/GCE that the rGO is synthesized in a typical crumpled and wrinkled nanosheet structure. The electrochemical reduction could remove most of the oxygen groups and sp³ carbon to the formation of rGO because of the increase of π - π interaction between rGO nanosheets [30]. The morphology of MnO₂/rGO/GCE in Figure 1c displays the vertical growth of MnO₂ nanoplates on agglomerated crumpled rGO nanosheets which surrounded the MnO₂ nanostructures. It is observed that the electrodeposition of MnO₂ nanostructures on the surface of rGO nanosheets to some extent prevents the stacking of rGO sheets because of van der Waals interactions, resulting in a large electroactive area on the GCE surface and rich porous structure for transferring reactants and products [31]. Moreover, the high porous and sharp tips of MnO₂ nanoplates on rGO nanosheets could provide the high surface-to-volume ratio and numerous of electro-active sites and hot spots which effectively adsorb and interact with the analyte in an electrochemical cell and favorable for electrochemical sensing [32].

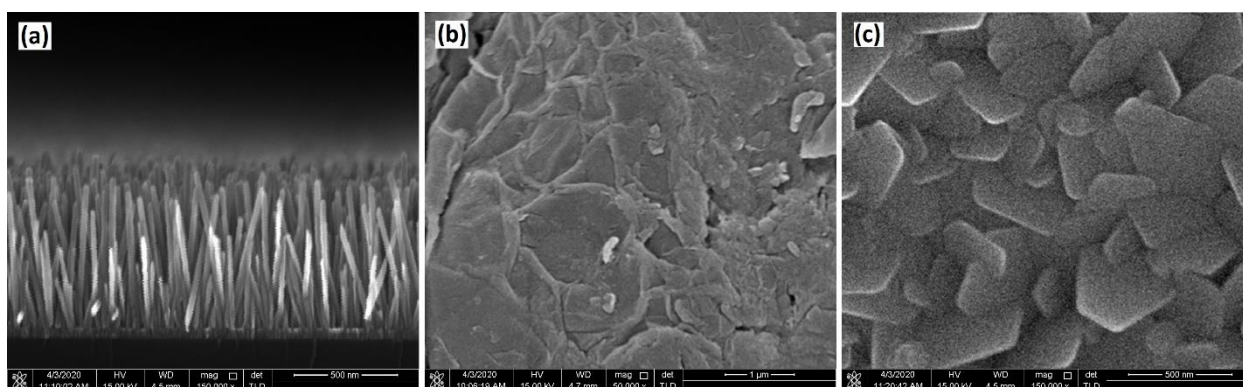


Figure 1. SEM image of (a) MnO₂/GCE, (b) rGO/GCE and (c) MnO₂/rGO/GCE.

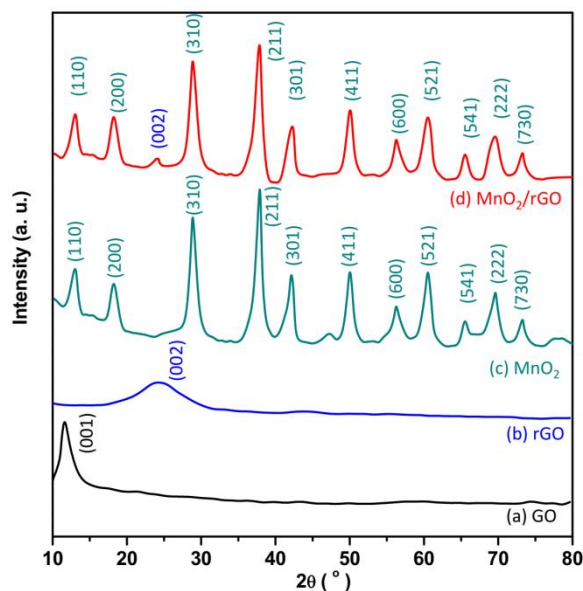


Figure 2. XRD patterns of powder of (a) GO, (b) rGO, (c) MnO_2 and (d) MnO_2/rGO .

Figure 2a depicts the XRD pattern of prepared GO with a sharp peak of (001) plane at 11.45° . The XRD pattern of rGO in Figure 2b shows a broad diffraction peak of graphite (002) at 24.42° that indicating that most of the oxygen functional groups in GO have been removed, and GO is deeply reduced into rGO [33, 34]. Figure 2c shows the XRD pattern of powder of electrodeposited MnO_2 nanostructures, indicating the strong diffraction peaks at 12.98° , 18.27° , 28.81° , 37.82° , 42.12° , 50.02° , 56.21° , 60.46° , 65.42° , 69.55° , and 73.65° which perfectly corresponding to formation of tetragonal crystalline of $\alpha\text{-MnO}_2$ with (110), (200), (310), (211), (301), (411), (600), (521), (541), (222), and (730) planes (JSPDF Card No. 44-0141), respectively. The XRD pattern of MnO_2/rGO in Figure 2d shows all diffraction peaks of MnO_2 and rGO which indicated to electrodeposition of MnO_2 nanostructures on rGO and maintain their crystalline structures.

3.2 Electrochemical studies

Figure 3 displays the CV curves of GCE, rGO/GCE, MnO_2/GCE and $\text{MnO}_2/\text{rGO}/\text{GCE}$ in 0.1 M PBS pH 7.0 containing 1 mM $[\text{Fe}(\text{CN})_6]^{3-/4-}$ as the redox probe in equal volume ratio at 10 mV/s scan rate. As seen, CV curves show the pair of redox peaks with peak potential separation ($\Delta E_p = |(E_{p,c} - E_{p,a})|$) of 0.09, 0.19, 0.12 and 0.09 V for GCE, rGO/GCE, MnO_2/GCE and $\text{MnO}_2/\text{rGO}/\text{GCE}$, respectively. As observed, the weak peaks and wide ΔE_p is observed for GCE, indicating the modification the GCE surface with the rGO and MnO_2 nanostructures enhanced the peak currents and decrease the ΔE_p values. In addition, it is observed that rGO role in enhancing the electrochemical current due to its high electrical conductivity with high electron mobility [35]. The rGO contains the abundant surface groups and residual sp^3 bonded carbon to oxygen, which improve the move of charge carriers by the hopping and produces a faster electron-transfer rate and a greater effective surface area than MnO_2 nanostructures [35, 36]. The higher peak current and lower ΔE_p are observed for

MnO₂/rGO/GCE that it is corresponding to the synergetic effect of rGO nanosheets and high porous and sharp tips of MnO₂ nanostructures [37]. Moreover, the effective surface area of electrodes is estimated using the Randles–Sevcik equation [38]:

$$I_p = 2.69 \times 10^5 n^{3/2} A D^{1/2} c v^{1/2} \quad (1)$$

Where I_p (A) is the peak current of the CV; n is the electron transfer number in the redox process ($n=1$); D is the diffusion coefficient of $\text{Fe}(\text{CN})_6^{3-/4-}$ ($7.6 \times 10^{-6} \text{ cm}^2/\text{s}$); A is the electroactive surface area of electrode; c is the redox probe concentration and v is the scan rate. Accordingly, the effective surface area of the bare GCE, rGO/GCE, MnO₂/GCE and MnO₂/rGO/GCE are obtained 0.093cm², 0.140cm², 0.148cm², and 0.173cm², respectively. Therefore, results illustrate to the higher electroactive surface area of MnO₂/rGO/GCE due to the high surface-to-volume ratio and numerous electro-active sites which is in agreement with the SEM results.

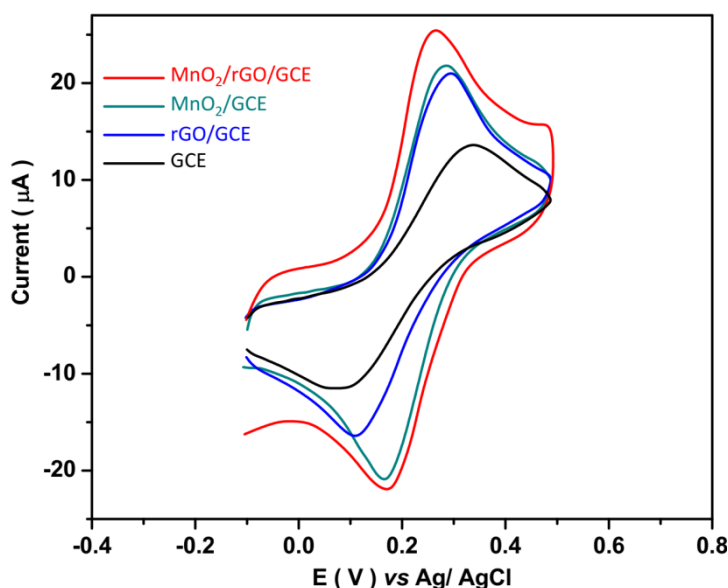


Figure 3. CV curves of GCE, rGO/GCE, MnO₂/GCE and MnO₂/rGO/GCE in 0.1M PBS containing 1mM $[\text{Fe}(\text{CN})_6]^{3-/4-}$ in equal volume ratio at 10mV/s scan rate.

Figure 4 shows the CV curves of all electrodes in 0.1M PBS at 20mV/s scan rate with and without 5 μM dopamine. As seen from Figure 4a, there are not any redox peaks for GCE and rGO/GCE but the CV curves of MnO₂/GCE and MnO₂/rGO/GCE show the anodic peaks at 0.46V and 0.36V that it is attributed to oxidation of Mn^{2+} to MnO_2 , and the cathodic peaks at 0.24V and 0.22V that it is related to the reduction of MnO_2 to Mn^{2+} [39, 40], respectively. When MnO₂ nanostructures are electrodeposited on rGO/GCE, the redox peaks of MnO₂ negatively shifts with a considerably increased peak current which can be associated with ultrathin-film nanoporous membranes of rGONanosheets on GCE surface [41, 42]. The electrochemical response of electrodes to

the addition of 5 μM dopamine is shown in Figure 4b. As observed, there are oxidation peaks at 0.24, 0.20, 0.14 and 0.11V with insufficient peak current for GCE and peak current of 0.50, 0.52 and 1.42 μA due to electrochemical oxidation of dopamine on rGO/GCE, MnO_2/GCE and $\text{MnO}_2/\text{rGO}/\text{GCE}$, respectively.

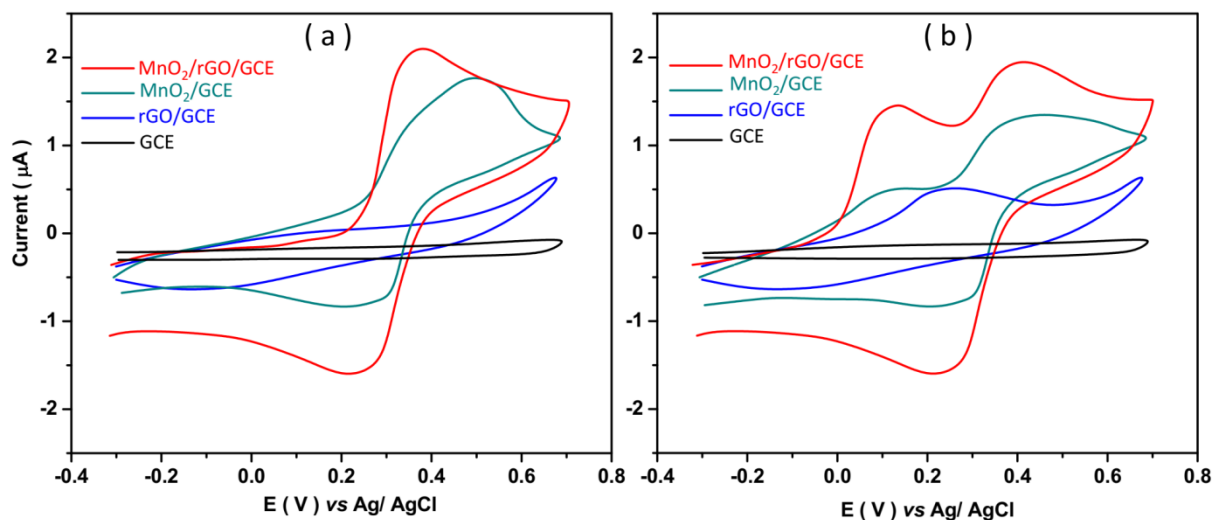


Figure 4. CV curves of GCE, rGO/GCE, MnO_2/GCE and $\text{MnO}_2/\text{rGO}/\text{GCE}$ in 0.1PBS at 20mV/s scan rate (a) without and (b) with 5 μM dopamine.

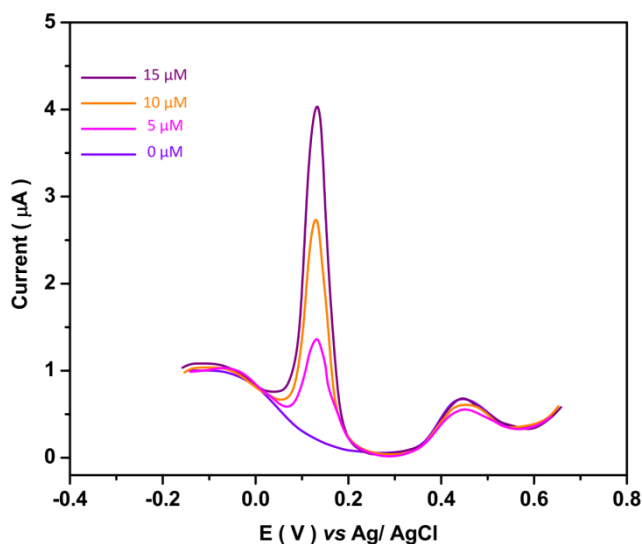


Figure 5. DPV curves of $\text{MnO}_2/\text{rGO}/\text{GCE}$ before and after addition of 5, 10 and 15 μM dopamine solutions in 0.1M PBS at 20mV/s scan rate.

Moreover, the redox peaks of MnO_2 were also observed for both MnO_2/GCE and $\text{MnO}_2/\text{rGO}/\text{GCE}$. The $\text{MnO}_2/\text{rGO}/\text{GCE}$ shows a higher current and lower potential than that other electrodes, and further electrochemical studies to the determination of dopamine were conducted on

MnO₂/rGO/GCE. Figure 5 displays the DPV curves of MnO₂/rGO/GCE before and after the addition of 5, 10 and 15 μ M dopamine solutions in 0.1M PBS at a 20mV/s scan rate. It shows that the oxidation peak at 0.11V is linearly increased with increasing the dopamine concentration, and the anodic peak of MnO₂ at 0.36V does not change. Therefore, the potential of 0.11V is considered as the oxidation potential of dopamine on MnO₂/rGO/GCE.

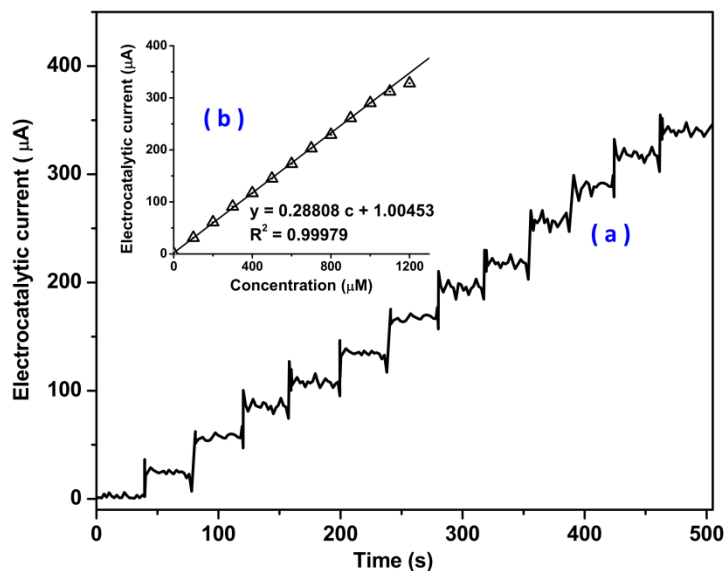


Figure 6. (a) Amperometry response and (b) obtained calibration plot of MnO₂/rGO/GCE in successive addition of dopamine in 0.1M PBS pH 7.0 at 0.11V with rotation speed of 1000rpm.

Table 1. Comparison between the performances of MnO₂/rGO/GCE and other reported graphene based dopamine sensors.

Electrode	Linear range (μ M)	Detection Limit (μ M)	Ref.
poly(o-phenylenediamine)/rGO	10-800	7.5	[43]
Exfoliated flexible graphite paper	0.5-35	0.01	[44]
Graphene flowers/Carbon fiber	0.7-45.21	0.5	[45]
Overoxidizedpolyimidazole/GO	12-278	0.63	[46]
Ionic liquid functionalized graphene/GCE	5-275	0.812	[47]
Pt NPs/rGO	10-170	0.25	[48]
NH ₂ -Fe ₃ O ₄ @ graphene sheets	0.2-38	0.126	[49]
rGO	0.5-60	0.5	[50]
Pd NPs/graphene/chitosan/GCE	0.5-200	0.1	[51]
Graphenenanosheets/Carbon paste electrode	2-1000	0.85	[52]
polypyrrole/rGO core-shell	0.06-8	0.006	[53]
Graphene modified electrode	2.5-100	0.5	[54]
Nitrogen doped graphene	0.5-170	0.25	[55]
Polyvinylpyrrolidone/Graphene	0.0005-1130	0.002	[56]
MnO ₂ /rGO/GCE	10-1100	0.002	This work

Studies the concentration effect of dopamine on MnO₂/rGO/GCE was conducted on amperometry technique in 0.1M PBS at 0.11V with the rotation speed of 1000rpm. Figure 6 displays the amperometry response and obtained calibration plot that reveals the linearly increasing the amperometric current with a concentration of dopamine in the range of 0 to 1100μM. Moreover, the limit of detection and sensitivity are obtained 0.002 μM and 0.28808μA/μM, respectively. The obtained limit of detection for the dopamine is found to be lower than the normal physiological level in the human body, and it signifies to the capability of the proposed sensor in biological application [57]. Table 1 presents the comparison between the performances of MnO₂/rGO/GCE and other reported graphene based dopamine sensors which indicated to lower detection limit and broad linear range of MnO₂/rGO/GCE than other sensors because of combining the advantages of MnO₂ rod-like nanostructures with rGO nanosheets and resulted in a large effective surface area and high electrical conductivity [58, 59].

For study the interference effect on determination of dopamine, the electrocatalytic amperometric response of MnO₂/rGO/GCE in 0.1 M PBS pH 7.0 at 0.11 V to addition 10 μM of dopamine and 70 μM of foreign species are shown in Table 2. Ascorbic acid is the most common substance that it has probability interference in physiological level (50 -70 μM) [60, 61]. Table 2 displays the insignificant electrocatalytic currents of the modified electrode to the addition ascorbic acid and other foreign species, and remarkable response to additions of dopamine, which demonstrated the foreign species in Table 2 do not any interference effect on determination dopamine and great selectivity of MnO₂/rGO/GCE using amperometry technique at 0.11 V.

Table 2. The amperometric responses of MnO₂/rGO/GCE in 0.1M PBS pH 7.0 at 0.11V for the addition of dopamine and foreign species

substance	Added (μM)	Electrocatalytic current response (μA)	RSD (%)
Dopamine	10	2.892	±0.017
Ascorbic acid	70	0.201	±0.010
Saccharose	70	0.090	±0.008
Glucose	70	0.071	±0.007
Uric acid	70	0.108	±0.011
Urea	70	0.069	±0.003
NH ₄ ⁺	70	0.089	±0.011
NO ₃ ⁻	70	0.071	±0.007
SO ₄ ⁻²	70	0.067	±0.005
CH ₃ CO ₂ ⁻	70	0.103	±0.010
PO ₄ ³⁻	70	0.088	±0.003
CO ₃ ⁻²	70	0.097	±0.011
Ca ²⁺	70	0.110	±0.009
Mg ²⁺	70	0.076	±0.007
Fe ³⁺	70	0.080	±0.003
Fe ²⁺	70	0.077	±0.004
Cu ²⁺	70	0.080	±0.008
K ⁺	70	0.093	±0.003

The practical feasibility of MnO₂/rGO/GCE as a dopamine sensor was evaluated in dopamine hydrochloride injection as a pharmaceutical product. Recognized concentrations of dopamine were pointed into the corresponding injection and amperometry measurements were carried out in 0.1M PBS pH 7.0 at 0.11V. Figure 7 indicates the obtained amperometric response and calibration plot which illustrated dopamine concentration in initial dopamine hydrochloride injection is 38.97 mg/mL that it shows good agreements between the electrochemical analysis and clinical laboratory data of dopamine hydrochloride injection (40 mg/mL). In addition, as observed in Table 3, the recovery (> 98.2%) and relative standard derivation (<3.91%) are acceptable. Therefore, the proposed dopamine sensor can be used as a precise and reliable sensor in complicated pharmaceutical samples.

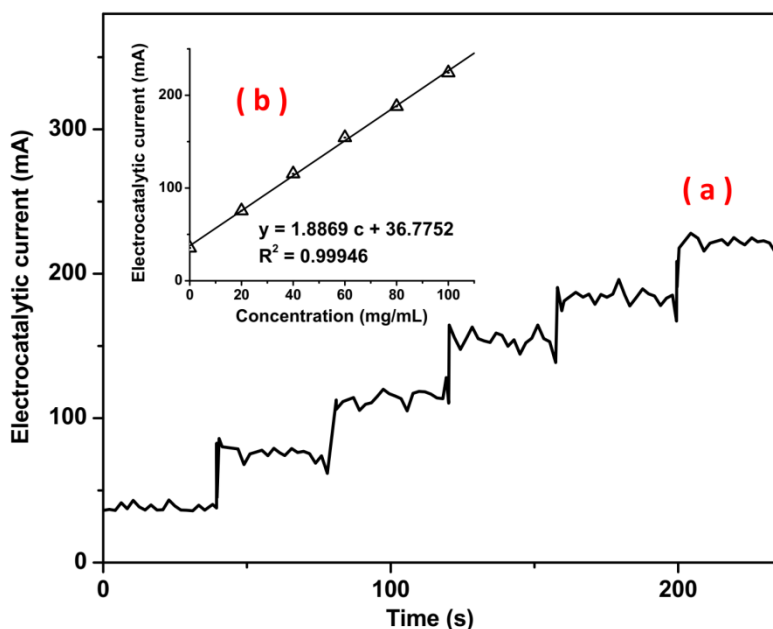


Figure 7. (a) The amperometry measurements and (b) the calibration plot of MnO₂/rGO/GCE in 0.1M PBS pH7.0 at 0.11V in successive additions 20 mg/mL dopamine solution.

Table 2. Analytical results of analysis real samples.

Sample	Added (mg/mL)	Measured (mg/mL)	Recovery (%)	Relative standard derivation (%)
dopamine hydrochloride injection	20.0	19.8	99.0	2.51
	40.0	39.6	99.0	3.14
	60.0	58.9	98.2	3.33
	100.0	98.8	98.8	3.91

4. CONCLUSIONS

This study presented fabrication of the electrochemical dopamine sensor based on nanostructured MnO₂/rGO/GCE in the pharmaceutical sample. The modified Hummers method was used for synthesis GO which modified GCE, and then reduced using the electrochemical method. Then, MnO₂ nanostructures were electrodeposited on rGO/GCE. Morphological and structural results showed the vertical growth of tetragonal crystalline of α -MnO₂ nanoplates on crumpled rGO nanosheets. The results of electrochemical studies indicated that the linear range, detection limit and sensitivity of MnO₂/rGO/GCE as dopamine sensor were obtained at 0 to 1100 μ M, 0.002 μ M and 0.28808 μ A/ μ M, respectively. Moreover, results indicated to the great selectivity and precise and reliable performance of MnO₂/rGO/GCE as a dopamine sensor in complicated pharmaceutical samples.

ACKNOWLEDGEMENT

The research is supported by: Key project of traditional Chinese medicine research in Henan Province: Study on treatment of senile dementia with Shenghua Decoction based on mTOR pathway (No.20-21zy1042); General subject of traditional Chinese medicine research in Henan Province: Proteomic study on the inhibition of xuanfuhua Decoction on hepatoma cell line 7721 and its molecular mechanism (No.20-21zy2124).

References

1. T.A. Ala, R.C. Doss and C.J. Sullivan, *Journal of Alzheimer's Disease*, 6 (2004) 503.
2. Q. Hu, W. Zhang, Q. Yin, Y. Wang and H. Wang, *Spectrochimica Acta Part A: Molecular and Biomolecular Spectroscopy*, 244 (2021) 118864.
3. X. Li, T. Shi, B. Li, X. Chen, C. Zhang, Z. Guo and Q. Zhang, *Materials & Design*, 183 (2019) 108152.
4. Z. Dai, J. Xie, Z. Chen, S. Zhou, J. Liu, W. Liu, Z. Xi and X. Ren, *Chemical Engineering Journal*, 410 (2021) 128341.
5. Z. Chen, H. Zhang, X. He, G. Fan, X. Li, Z. He, G. Wang and L. Zhang, *BioResources*, 16 (2021) 2644.
6. Z. Dai, S. Guo, Y. Gong and Z. Wang, *Ceramics International*, 47 (2021) 6535.
7. X. Wang, Z. Feng, B. Xiao, J. Zhao, H. Ma, Y. Tian, H. Pang and L. Tan, *Green Chemistry*, 22 (2020) 6157.
8. Y. Yang, H. Chen, X. Zou, X.-L. Shi, W.-D. Liu, L. Feng, G. Suo, X. Hou, X. Ye and L. Zhang, *ACS applied materials & interfaces*, 12 (2020) 24845.
9. L. Zhang, J. Zheng, S. Tian, H. Zhang, X. Guan, S. Zhu, X. Zhang, Y. Bai, P. Xu and J. Zhang, *Journal of Environmental Sciences*, 91 (2020) 212.
10. N. Zhao, L. Deng, D. Luo and P. Zhang, *Applied Surface Science*, 526 (2020) 146696.
11. P. Dong, T. Zhang, H. Xiang, X. Xu, Y. Lv, Y. Wang and C. Lu, *Journal of Materials Chemistry B*, 9 (2021) 958.
12. G. Koch, C. Motta, S. Bonni, M.C. Pellicciari, S. Picazio, E.P. Casula, M. Maiella, F. Di Lorenzo, V. Ponzio, C. Ferrari, E. Scaricamazza, C. Caltagirone and A. Martorana, *JAMA network open*, 3 (2020) e2010372.
13. Z. Wang, T. Zhang, L. Pi, H. Xiang, P. Dong, C. Lu and T. Jin, *Colloids and Surfaces B: Biointerfaces*, 198 (2021) 111480.

14. K. Yang, Q. Liu, Y. Zheng, H. Yin, S. Zhang and Y. Tang, *Angewandte Chemie*, 133 (2021) 6396.
15. M. Zhang, L. Zhang, S. Tian, X. Zhang, J. Guo, X. Guan and P. Xu, *Chemosphere*, 253 (2020) 126638.
16. M. De Marco and A. Venneri, *Journal of Alzheimer's Disease*, 63 (2018) 167.
17. Z. Dai, J. Xie, X. Fan, X. Ding, W. Liu, S. Zhou and X. Ren, *Chemical Engineering Journal*, 397 (2020) 125520.
18. A.M. El-Zohry and E.Y. Hashem, *Journal of Spectroscopy*, 2013 (2013) 260376.
19. Z.T. Al-thagafi and M. Awad, *International Journal of Electrochemical Science*, 15 (2020) 5860.
20. B. Zhang, Q. Wu, B. Li, X. Tang, F. Ju, Q. Yang, Wang2, Q. , Zhou2 and Y.L. , *International Journal of Electrochemical Science*, 15 (2020) 137.
21. Z. Wei, Y. Hu, Q. Tu, S. Cui, Y. Li, Y. Gan, G. Li, H. Yang and S. Li, *International Journal of Electrochemical Science*, 16 210612.
22. Z. Ni, X. Cao, X. Wang, S. Zhou, C. Zhang, B. Xu and Y. Ni, *Coatings*, 11 (2021) 749.
23. M. Zhang, X. Song, X. Ou and Y. Tang, *Energy Storage Materials*, 16 (2019) 65.
24. K.M. AlAqad, R. Suleiman, O.C.S. Al Hamouz and T.A. Saleh, *Journal of Molecular Liquids*, 252 (2018) 75.
25. X. Zhang, Y. Tang, F. Zhang and C.S. Lee, *Advanced Energy Materials*, 6 (2016) 1502588.
26. E. Aliyev, V. Filiz, M.M. Khan, Y.J. Lee, C. Abetz and V. Abetz, *Nanomaterials*, 9 (2019) 1180.
27. P.K. Aneesh, S.R. Nambiar, T.P. Rao and A. Ajayaghosh, *Analytical Methods*, 6 (2014) 5322.
28. N. Cherchour, C. Deslouis, B. Messaoudi and A. Pailleret, *Electrochimica Acta*, 56 (2011) 9746.
29. A. Idris, J. Mafa, N. Mabuba and O. Arotiba, *Russian Journal of Electrochemistry*, 53 (2017) 170.
30. S. Phetsang, P. Kidkhunthod, N. Chanlek, J. Jakmune, P. Mungkornasawakul and K. Ounnunkad, *Scientific reports*, 11 (2021) 1.
31. R. Nie, J. Shi, S. Xia, L. Shen, P. Chen, Z. Hou and F.-S. Xiao, *Journal of Materials Chemistry*, 22 (2012) 18115.
32. J. Wang, B. Yang, F. Gao, P. Song, L. Li, Y. Zhang, C. Lu, M.C. Goh and Y. Du, *Nanoscale research letters*, 14 (2019) 1.
33. M.R. Thalji, G.A. Ali, S.P. Lee and K.F. Chong, *Chem. Adv. Mater.*, 4 (2019) 17.
34. R. Wang, Y. Yuan, J. Zhang, X. Zhong, J. Liu, Y. Xie, S. Zhong and Z. Xu, *Journal of Power Sources*, 501 (2021) 230006.
35. A.T. Smith, A.M. LaChance, S. Zeng, B. Liu and L. Sun, *Nano Materials Science*, 1 (2019) 31.
36. N.S. Ahmed, O. Azizi, A. El-Boher, J. Gahl and S. Bok, *ECS Journal of Solid State Science and Technology*, 7 (2018) M173.
37. R. Savari, H. Savaloni, S. Abbasi and F. Placido, *Sensors and Actuators B: Chemical*, 266 (2018) 620.
38. Z. Savari, S. Soltanian, A. Noorbakhsh, A. Salimi, M. Najafi and P. Servati, *Sensors and Actuators B: Chemical*, 176 (2013) 335.
39. S. Nijjer, J. Thonstad and G. Haarberg, *Electrochimica acta*, 46 (2000) 395.
40. K. Kim, G. Daniel, V.G. Kessler, G.A. Seisenbaeva and V.G. Pol, *Nanomaterials*, 8 (2018) 608.
41. B. Mekassa, M. Tessema, B.S. Chandravanshi, P.G. Baker and F.N. Muya, *Journal of Electroanalytical Chemistry*, 807 (2017) 145.
42. H. Savaloni, R. Savari and S. Abbasi, *Current Applied Physics*, 18 (2018) 869.
43. X. Liu, H. Zhu and X. Yang, *RSC Advances*, 4 (2014) 3706.
44. W. Cai, T. Lai, H. Du and J. Ye, *Sensors and Actuators B: Chemical*, 193 (2014) 492.

45. J. Du, R. Yue, F. Ren, Z. Yao, F. Jiang, P. Yang and Y. Du, *Biosensors and bioelectronics*, 53 (2014) 220.
46. X. Liu, L. Zhang, S. Wei, S. Chen, X. Ou and Q. Lu, *Biosensors and Bioelectronics*, 57 (2014) 232.
47. C. Wang, P. Xu and K. Zhuo, *Electroanalysis*, 26 (2014)
48. T.-Q. Xu, Q.-L. Zhang, J.-N. Zheng, Z.-Y. Lv, J. Wei, A.-J. Wang and J.-J. Feng, *Electrochimica Acta*, 115 (2014) 109.
49. D. Wu, Y. Li, Y. Zhang, P. Wang, Q. Wei and B. Du, *Electrochimica Acta*, 116 (2014) 244.
50. L. Yang, D. Liu, J. Huang and T. You, *Sensors and Actuators B: Chemical*, 193 (2014) 166.
51. X. Wang, M. Wu, W. Tang, Y. Zhu, L. Wang, Q. Wang, P. He and Y. Fang, *Journal of Electroanalytical Chemistry*, 695 (2013) 10.
52. M. Bagherzadeh and M. Heydari, *Analyst*, 138 (2013) 6044.
53. T. Qian, S. Wu and J. Shen, *Chemical Communications*, 49 (2013) 4610.
54. X. Ma, M. Chao and Z. Wang, *Analytical Methods*, 4 (2012) 1687.
55. Z.-H. Sheng, X.-Q. Zheng, J.-Y. Xu, W.-J. Bao, F.-B. Wang and X.-H. Xia, *Biosensors and Bioelectronics*, 34 (2012) 125.
56. Q. Liu, X. Zhu, Z. Huo, X. He, Y. Liang and M. Xu, *Talanta*, 97 (2012) 557.
57. L. Durai and S. Badhulika, *Materials Science and Engineering: C*, 109 (2020) 110631.
58. F. Chahshouri, H. Savaloni, E. Khani and R. Savari, *Journal of Micromechanics and Microengineering*, 30 (2020) 075001.
59. H. Savaloni, E. Khani, R. Savari, F. Chahshouri and F. Placido, *Applied Physics A*, 127 (2021) 1.
60. S.R. Ali, R.R. Parajuli, Y. Ma, Y. Balogun and H. He, *The Journal of Physical Chemistry B*, 111 (2007) 12275.
61. S.F. Rahman, K. Min, S.-H. Park, J.-H. Park, J.C. Yoo and D.-H. Park, *Biotechnology and Bioprocess Engineering*, 21 (2016) 627.